Journal of Sea Research 175 (2021) 102085

Contents lists available at ScienceDirect

Journal of Sea Research

journal homepage: www.elsevier.com/locate/seares

Characteristics of sediment resuspension on a deep abyssal plain in the Eastern Tropical Pacific Ocean

Minkyoung Kim [a,b], Hyung Jeek Kim [c], Ara Ko [a,b], Chan Min Yoo [b], Se-Jong Ju [b], Jeomshik Hwang [a,*]

[a] School of Earth and Environmental Sciences/Research Institute of Oceanography, Seoul National University, Seoul 08826, South Korea
[b] Korea Institute of Ocean Science & Technology, Pusan 49111, South Korea
[c] Korea Institute of Ocean Science & Technology, Jeju 63349, South Korea

ARTICLE INFO

Keywords:
Sediment trap
Radiocarbon
Abyssal plain
Sinking particles
Eastern Tropical Pacific Ocean

ABSTRACT

We examined the biogenic and lithogenic particle composition and radiocarbon content of sinking particulate organic carbon to investigate sediment resuspension and its contribution to sinking particles on the deep abyssal plain of the Eastern Tropical Pacific Ocean. Samples were collected using sediment traps from August 2011 to July 2012 at depths of 4500 and 4950 m (50 m above the seafloor); above and within the benthic nepheloid layer (BNL), respectively. Biogenic particles derived from export production were the major source of sinking particles and their flux showed a unimodal temporal distribution, with larger values between February and April. At a depth of 4500 m, the lithogenic material flux was slightly greater than, or similar to, the flux of atmospheric dust deposition. In comparison, lithogenic material and excess Mn consistently showed a greater contribution to resuspended particles at 4950 m. The lithogenic material flux was proportional to the biogenic flux. These observations imply that resuspended particles exist at a background concentration in the BNL throughout the year, and are scavenged by sinking biogenic particles, especially during the high flux period.

1. Introduction

Particle sedimentation processes at the continental margins are influenced by the resuspension of clay- and silt-sized particles from the seafloor, and their lateral transport by strong shelf currents and tidal activity (Hollister and McCave, 1984; Inthorn et al., 2006; Karakaş et al., 2006; McCave and Hall, 2006). In the open ocean, the majority of particles sinking to the deep ocean are considered to originate from primary production, along with minute amounts derived from aeolian dust (Martin et al., 1987; Buesseler, 1998; Ducklow et al., 2001). Attenuation of the sinking particle flux during vertical transit has been studied extensively (Martin et al., 1987; Armstrong et al., 2001; Buesseler et al., 2008; Buesseler and Boyd, 2009; Marsay et al., 2015). The vertical distribution of the suspended particle concentration in the water column generally shows high concentrations in the surface water layer, minimum concentrations in the middle layer, and somewhat elevated values near the seafloor (Gardner et al., 1985). A recent sediment trap study has shown a similar vertical trend in the lithogenic particle flux (Kim et al., 2020). However, sediment resuspension and its contribution to sinking particles on the abyssal plain has received less attention.

A long-term sediment trap study began in 2003 at Station KOMO, which is a deep-sea mooring site located on the abyssal plain of the Eastern Tropical Pacific (Fig. 1). The station is located at 10°N in the thermocline ridge area where temporal fluctuations in primary production and zooplankton abundances are influenced by the seasonal migration of the Intertropical Convergence Zone and ENSO (El Niño–Southern Oscillation) conditions (Blackburn et al., 1970; El-Sayed and Taguchi, 1979; Pennington et al., 2006; Kim et al., 2010, 2011, 2019). One motivation for studying this site was to provide reference data for comparison with potential future disturbance at this site as a result of Mn nodule mining (Kim et al., 2015). Kim et al. (2015) investigated the use of the ratio of lithogenic material to particulate organic carbon (POC) in sinking particles as a tracer of sediment resuspension. They proposed that the radiocarbon content of the sinking POC was useful for estimating the contribution of sediment resuspension to sinking particles. However, they did not validate these indicators against real data.

Station KOMO is located on a calm abyssal plain with low surface

* Corresponding author at: School of Earth and Environmental Sciences, Seoul National University, Seoul 151-742, South Korea.
E-mail address: jeomshik@snu.ac.kr (J. Hwang).

https://doi.org/10.1016/j.seares.2021.102085
Received 20 May 2021; Received in revised form 4 July 2021; Accepted 10 July 2021
Available online 14 July 2021

eddy kinetic energy (Gardner et al., 2018). The site is >2500 km away from the nearest continental margin of the American continents, East Pacific Rise, and Hawaiian islands. This region is expected to be minimally influenced by the Asian dust flux (Duce, 2014). In a survey of the global distribution of the benthic nepheloid layer (BNL), Gardner et al. (2018) reported no significant BNL and low particle concentrations (<10 $\mu g L^{-1}$) in this region. We investigated the characteristics of sinking particles near the seafloor on this supposedly calm abyssal plain. To understand the existing status of sediment resuspension, we examined metal-based properties, such as lithogenic material content and excess Mn, in addition to the radiocarbon isotope ratio of sinking POC.

2. Methods

Samples of the sinking particles were collected using sediment traps (PARFLUX Mark 78G-21; McLane; conical type with 0.5 m^2 funnel opening) between August 2011 and July 2012, from water depths of 4500 and 4950 m (50 m above the seafloor) at the deep-sea mooring site of Station KOMO (10.5°N, 131.33°W; 5005 m; Fig. 1). The fluxes of total particles, POC, and $CaCO_3$ have been reported elsewhere (Kim et al., 2019).

The analytical methods used to determine the total particle flux, total carbon, inorganic carbon, and organic carbon contents are described in Kim et al. (2011, 2019). In brief, the total carbon content was determined using an elemental analyzer (Flash EA1112, Thermo Fisher Scientific, UK) with an analytical uncertainty of <3% (relative standard deviation; RSD). The particulate inorganic carbon (PIC) content was determined using coulometric titration (CO_2 coulometer, model CM5014 UIC, Inc., USA) with a 2% RSD. The organic carbon content was estimated as the difference between the total and inorganic carbon contents. The $CaCO_3$ content was estimated by multiplying the PIC content by 8.33 (the ratio of $CaCO_3$ to carbon). The opal content was estimated by multiplying the biogenic Si content by 2.4, which was determined by subtracting the lithogenic Si (3.5 × Al) from the measured total Si content (Honjo et al., 1995). The lithogenic material content was estimated by multiplying the Al content by 12.15 (Taylor, 1964). The contents of Al, Ca, Si, and Mn were determined using an ICP-AES (Optima 8300, PerkinElmer, Inc., USA) at the Korea Basic Science Institute, with an RSD of <2%, based on blind duplicate analysis.

To obtain sufficient material for radiocarbon and metal analysis

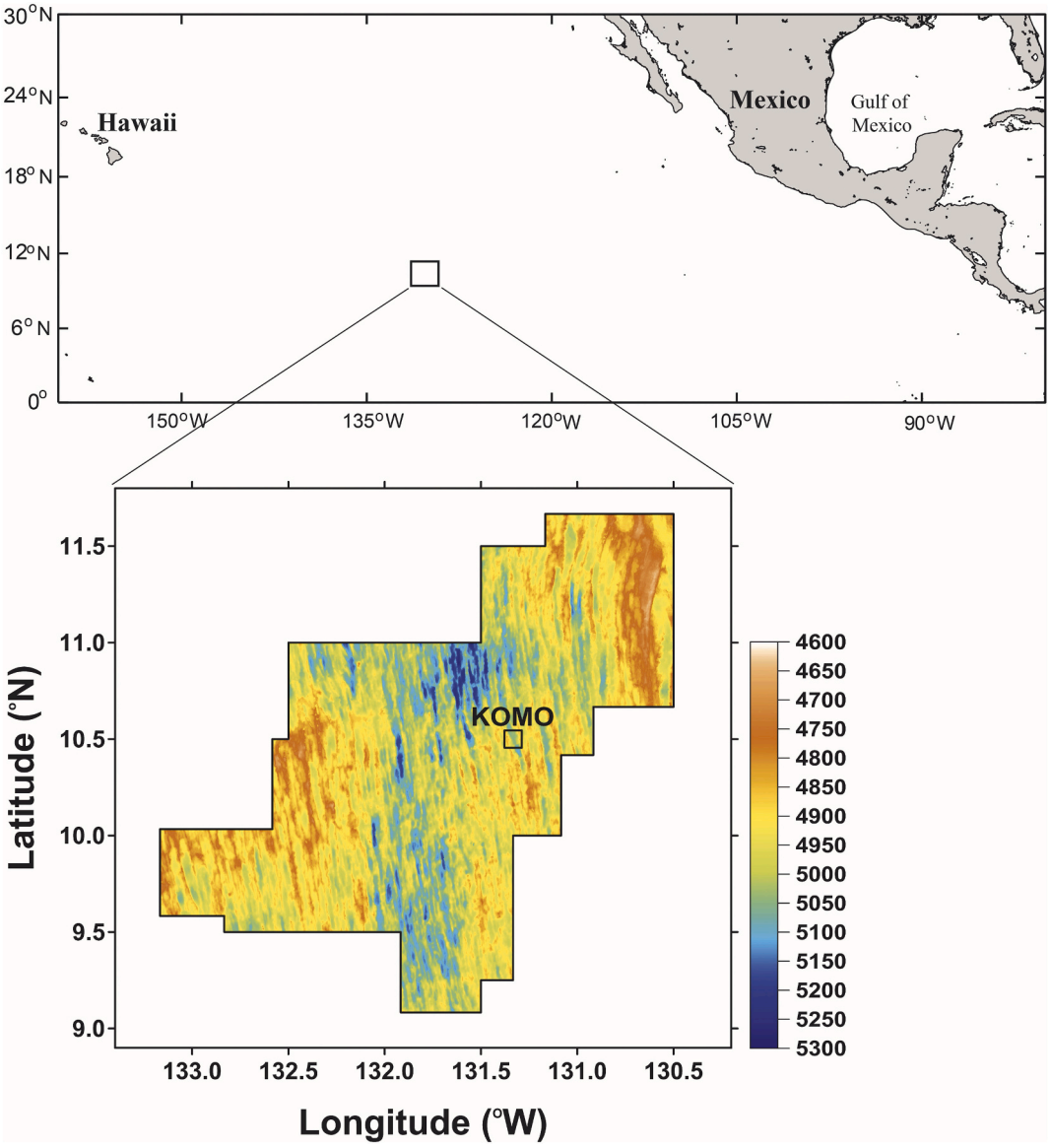

Fig. 1. Bathymetric map showing the location of Station KOMO in the Tropical Pacific. Colour bar indicates water depth (m). (For interpretation of the references to color in this figure legend, the reader is referred to the web version of this article.)

Table 1
Sampling times, cup opening intervals, fluxes of total particles and POC, contents of biogenic and lithogenic components, and radiocarbon values of sinking particles collected from the depths of 4500 and 4950 m. Fluxes of total particles, POC, and $CaCO_3$ are from Kim et al. (2019). The mixing ratios show how samples were mixed for radiocarbon analysis and other components. 'Avg.' indicates the sampling duration-weighted annual mean of each values.

Cup #	Cup opening date (mm/dd/yy)	Interval (days)	Particle flux (mg m^{-2} d^{-1})	POC flux (mgC m^{-2} d^{-1})	POC (%)	$CaCO_3$ (%)	mixing ratio (%)	$\Delta^{14}C$ (‰)	mixing ratio (%)	Opal (%)	Lithogenic material (%)	excess Mn (ppm)	$Litho_{resusp}$
4500 m													
1	08/05/11	27	14	1.6	12	38	16	−12	15	36	5.3	109	0.7
2	09/01/11	30	17	2.1	13	40	19		20				
3	10/01/11	31	22	2.7	12	34	29		30				
4	11/01/11	30	26	2.3	9.1	36	36		34				
5	12/01/11	31	39	3.4	8.8	33	100	−5	39	39	3.3	62	1.2
6	01/01/12	31	47	4.2	8.8	42	100	−4	61				
7	02/01/12	29	127	11	8.9	39	100	12	100	36	2.0	29	2.2
8	03/01/12	7	56	5.0	8.9	46	14	−6	15	20	2.9	37	1.4
9	03/08/12	7	89	7.1	7.9	54	18		17				
10	03/15/12	7	94	6.1	6.5	66	29		28				
11	03/22/12	7	76	5.0	6.6	64	24		19				
12	03/29/12	7	78	6.5	8.3	61	14		22				
13	04/05/12	7	67	4.0	6.0	67	32	−25	35	22	3.5	53	1.6
14	04/12/12	7	86	6.2	7.3	58	22		33				
15	04/19/12	7	49	3.9	8.1	53	27		18				
16	04/26/12	7	41	3.5	8.5	52	19		14				
17	05/03/12	7	39	3.0	7.8	55	9	−17	19	28	4.0	63	0.8
18	05/10/12	7	36	2.7	7.6	56	8		11				
19	05/17/12	15	44	3.8	8.6	49	83		70				
20	06/01/12	30	27	2.2	8.0	55	61	10	66	21	3.3	72	0
21	07/01/12	31	18	2.2	12	45	39		34				
Avg.			43	3.8	10	44		−15		31	3.9	73	0.9
4950 m													
1	08/05/11	27	16	1.8	11	28	13	5	15	33	20	479	4.1
2	09/01/11	30	21	2.1	10	28	18		24				
3	10/01/11	31	20	2.2	11	29	28		26				
4	11/01/11	30	29	2.3	8.1	29	41		34				
5	12/01/11	31	38	3.0	7.7	24	100	−4	100	44	15	315	5.4
6	01/01/12	31	54	4.5	8.3	31	100	ND	100	35	13	286	6.9
7	02/01/12	29	104	9.4	9.1	34	100	15	100	39	7	135	7.2
8	03/01/12	7	74	7.0	9.4	36	13	−13	20	26	11	198	7.7
9	03/08/12	7	70	6.0	8.7	41	19		19				
10	03/15/12	7	73	5.0	6.8	53	25		27				
11	03/22/12	7	100	8.1	8.1	47	32		21				
12	03/29/12	7	71	5.6	8.0	47	11		14				
13	04/05/12	7	79	5.7	7.3	47	53	3	35	26	14	254	7.4
14	04/12/12	7	55	4.3	7.9	43	23		29				
15	04/19/12	7	21	1.4	6.7	46	12		17				
16	04/26/12	7	51	4.1	7.9	36	12		18				
17	05/03/12	7	15	1.3	8.9	39	7	4	18	32	14	283	2.9
18	05/10/12	7	26	2.4	9.3	37	2		4				
19	05/17/12	15	30	2.5	8.3	37	92		78				
20	06/01/12	30	19	1.5	8.1	45	79	0	63	29	18	440	2.0
21	07/01/12	31	15	1.1	7.1	42	21		37				
Avg.			40	3.4	8.7	35		8		33	16	354	4.9

(Table 1), it was necessary to combine some samples. The ratio of each combined sample was maintained to be proportional (at least approximately) to the total particle fluxes, except for samples #17–#19 at both sampling depths, and samples #20 and #21 at 4950 m for the radiocarbon analysis (Table 1).

Details of the radiocarbon analysis are presented in Kim et al. (2017). In brief, each sample was weighed into an Ag cup and fumigated with concentrated HCl in a desiccator for ~20 h (Hedges and Stern, 1984; Komada et al., 2008). The samples were combusted in evacuated quartz tubes with CuO at 850 °C for 4 h. The resultant CO_2 gases were analyzed for radiocarbon and stable carbon isotope ratios at the National Ocean Sciences Accelerator Mass Spectrometry Facility at Woods Hole Oceanographic Institution (NOSAMS WHOI) following standard techniques (McNichol et al., 1994). An uncertainty of <10‰ for $\Delta^{14}C$ measurements on these types of samples was determined through multiple duplicate analyses in our laboratory. Two samples (sample #7 from 4500 m and 4950 m) were also measured for radiocarbon at ETH Zürich as duplicates. These samples were fumigated with HCl in a desiccator for 3 d at 70 °C, and then fumigated with NaOH pellets at 70 °C for >3 d to remove HCl vapor. The radiocarbon content was measured on a gas ion source MICADAS (Mini Carbon Dating System) accelerator mass spectrometer (AMS) at the Laboratory for Ion Beam Physics at ETH Zürich (Christl et al., 2013; McIntyre et al., 2017). The $\Delta^{14}C$ values from these two duplicate samples were identical within the measurement uncertainty (+12‰ and +14‰ for sample #7 at 4500 m and +15‰ and +11‰ for sample #7 at 4950 m; we used the values obtained from WHOI for consistency). Sodium borate-buffered 10% formalin solution was added as a preservative to the sediment trap sampling cups. We believe that rinsing the samples with ultrapure water three times and then freeze-drying under vacuum reduces the effect of the formalin on the radiocarbon analysis to negligible levels (Honda et al., 2000; Otosaka et al., 2008).

Light attenuation results were obtained on July 13th 2010 using a CTD system (SBD 911plus CTD, SEA-BIRD SCIENTIFIC, USA) equipped with a transmissometer (C-Star transmissometer, SEA-BIRD SCIENTIFIC, USA). The dust deposition flux was obtained from the Modern-Era Retrospective analysis for Research and Applications version 2 (MERRA-2) model developed and maintained by the NASA Goddard Earth Sciences Data and Information Services Center (GES DISC; Acker and Leptoukh, 2007). The data were averaged over the 10–11°N and 130–133°W region.

3. Results

The total particle flux at 4500 m ranged between 14 and 127 mg m^{-2} d^{-1}, with the highest value observed in February (Fig. 2; Table 1). The total particle flux at 4950 m ranged between 15 and 104 mg m^{-2} d^{-1} and exhibited a similar temporal variation to that seen at 4500 m. The annual average total particle flux (sampling duration-weighted) was 15.7 and 14.3 g m^{-2} yr^{-1} (equivalent to an average daily flux of 43 and 40 mg m^{-2} d^{-1}) at 4500 and 4950 m, respectively. The POC flux ranged from 1.6 to 11.4 mg C m^{-2} d^{-1} and from 1.1 to 9.4 mg C m^{-2} d^{-1} at 4500 and 4950 m, respectively (Table 1). The annual average POC flux (sampling duration-weighted) was 3.8 and 3.4 mg C m^{-2} d^{-1} at 4500 and 4950 m, respectively. POC contents varied within narrow ranges, 8.8 ± 1.9 (1σ)% and 8.5 ± 1.2%, at 4500 and 4950 m, respectively (Table 1). The temporal variation of the POC flux was in phase with that of the total particle flux.

At 4500 m, the $CaCO_3$ and opal contents were similar from August to February (~40%: Fig. 2). However, from March, the opal content decreased while the $CaCO_3$ content increased. The opal flux at 4950 m was slightly less than that at 4500 m, by ~0.5% (arithmetic mean of seven results), indicating slow dissolution. In comparison, the $CaCO_3$ flux at 4950 m was less than that at 4500 m by ~8%, implying significant dissolution between these two depths.

The lithogenic material content ranged from 2.0% to 5.3% at 4500 m, and from 7% to 20% at 4950 m (Figs. 2–3; Table 1). The lowest values were observed in February and temporal variations at the two depths were similar. The excess Mn, [total Mn – Al × $(Mn/Al)_{ref}$, where $(Mn/Al)_{ref}$ = 0.0115; the average Mn/Al ratio of the upper crust (Taylor, 1964)], ranged from 29 to 109 ppm at 4500 m, and from 135 to 479 ppm at 4950 m (Fig. 3; Table 1).

The $\Delta^{14}C$ values of the sinking POC varied between −25‰ and 12‰ at 4500 m, and between −13‰ and 15‰ at 4950 m (Fig. 3; Table 1). The highest values were observed in February at both depths, and the lowest values were observed in April at 4500 m and in March at 4950 m (Fig. 3). The $\Delta^{14}C$ values at the both depths showed no well-defined trend, except that the highest values were observed in February at both depths when the biogenic particle flux was greatest. The $\Delta^{14}C$ values at both depths were comparable between December and March but differed at other times (student's *t*-test). The POC flux-weighted average $\Delta^{14}C$ values were −15‰ ± 13‰ and −8‰ ± 9‰ at 4500 and 4950 m, respectively.

4. Discussion

4.1. Contribution of resuspended sediment particles to sinking particles

The vertical distribution of light transmission shows a slight increase in the bottom ~300 m layer, which is an indication of the BNL although Gardner et al. (2018) reported no significant BNL around this region (Fig. 4). Our sampling at 4500 m occurred near the upper boundary of the BNL where the particle concentration would be most likely to be at a minimum. The average current speeds measured at 4550 m and 5000 m at the mooring site were 2.7 ± 1.9 and 4.0 ± 2.3 cm s^{-1}, respectively (Fig. 4), and were mostly below the threshold for local resuspension, 7 cm s^{-1} (Lampitt, 1985) although this threshold can be lower in the case

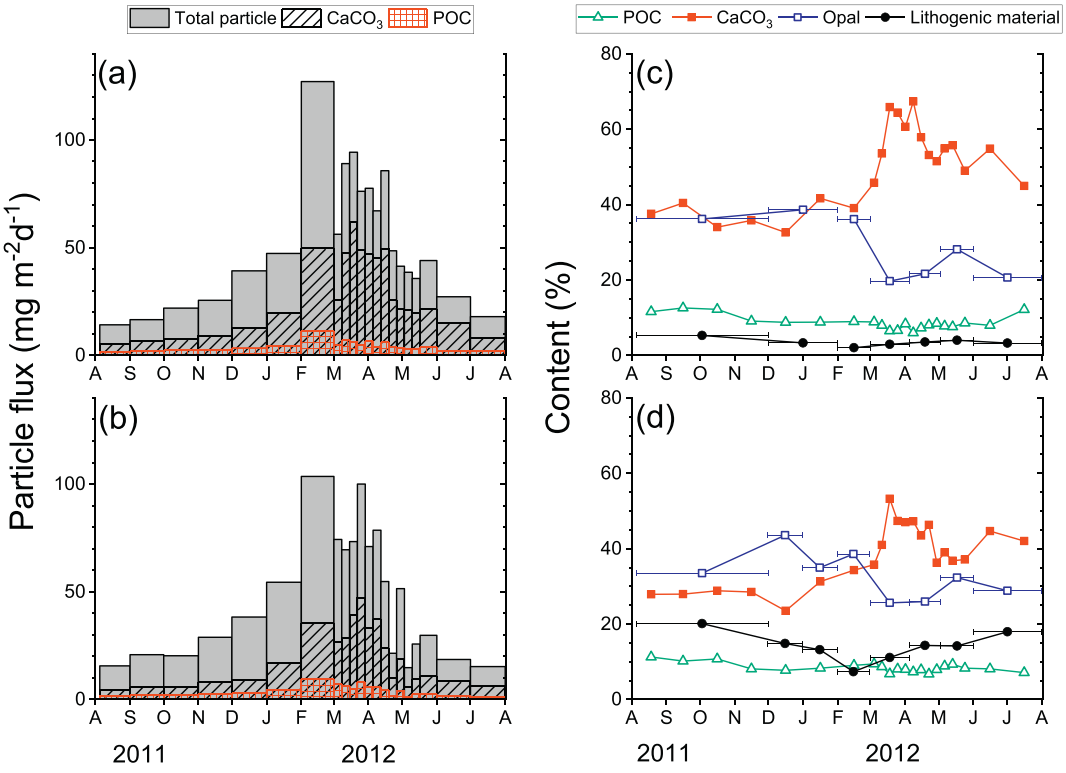

Fig. 2. Temporal variations in total particle flux (gray bars), $CaCO_3$ flux (hatched bars), and POC flux (checked red bars) at (a) 4500 m and (b) 4950 m. Note that the bars are not stacked and indicate the flux of each item. Temporal variations on the biogenic and lithogenic material contents at (c) 4500 m and (d) 4950 m Total particle, $CaCO_3$, POC and opal fluxes were published by Kim et al. (2019). (For interpretation of the references to colour in this figure legend, the reader is referred to the web version of this article.)

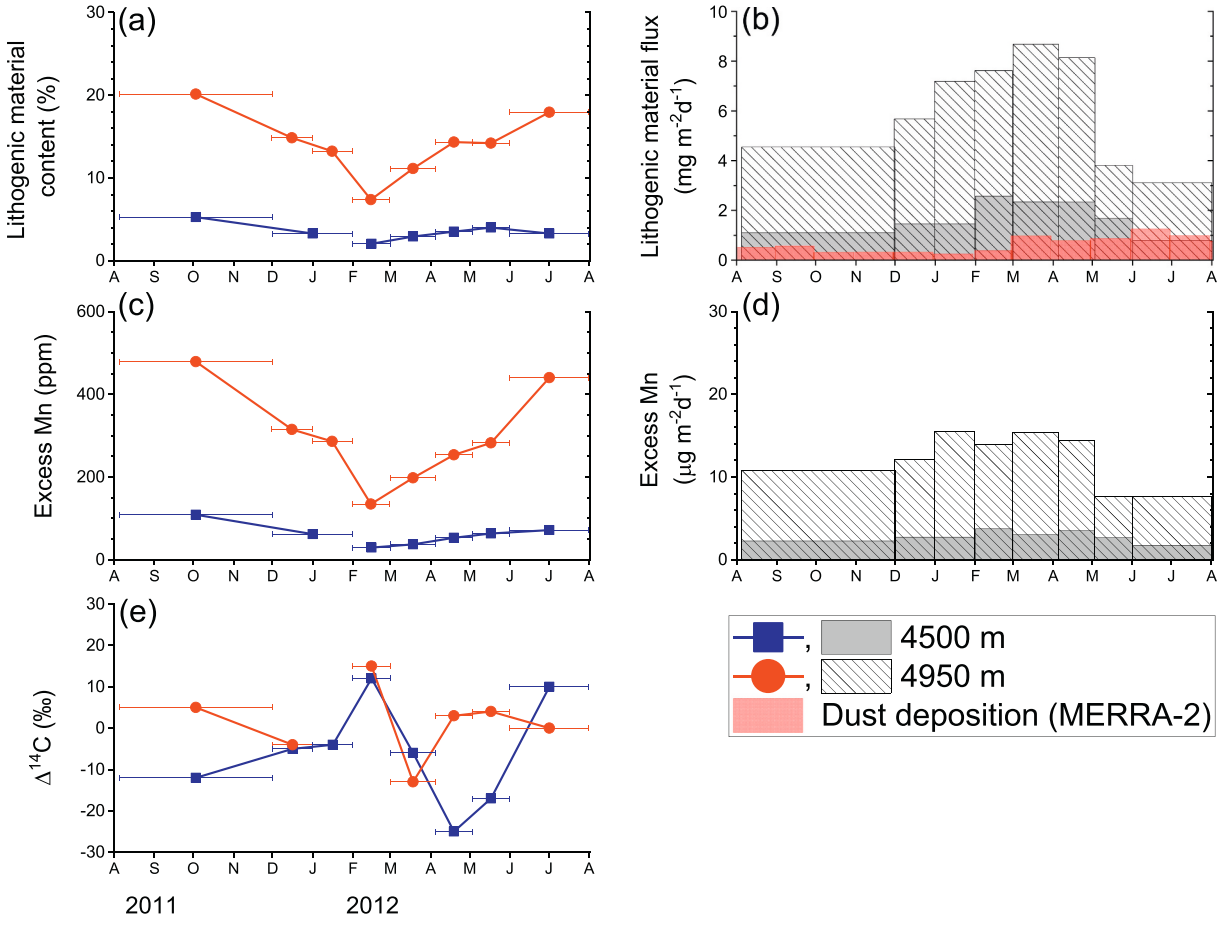

Fig. 3. Temporal variations in the lithogenic material (a) content and (b) flux, as well as in the excess Mn (c) contents and (d) flux, and in the (e) $\Delta^{14}C$ values at 4500 m and 4950 m. Note that the atmospheric dust deposition rate from the MERRA-2 model (red hatched bars) are also shown with the lithogenic material fluxes in (b). The bars in (b) and (d) are not stacked and indicate the flux of each item. (For interpretation of the references to colour in this figure legend, the reader is referred to the web version of this article.)

of turbulent flow. The strongest current speeds (4–8 cm s^{-1}) were observed in June and July at 5000 m (Fig. 4), during which period lithogenic material flux was at its smallest. Overall, the lithogenic material flux was not correlated with the current speed or direction (not shown). The temporal variation of the lithogenic material flux does not therefore appear to be directly related to the local current.

The rates of dust deposition obtained from the MERRA-2 model over the region bounded by 10–11°N and 130–133°W area during the study period were between 0.3 and 1.3 mg m^{-2} d^{-1}, with the larger values occurring between March and July (Fig. 3). The lithogenic material flux at 4500 m was more than twice the dust deposition, except for June and July when they were comparable. The lithogenic material flux at 4950 m was considerably greater than the dust deposition. Thus, changes in atmospheric dust deposition were not responsible for the observed seasonal variations in the lithogenic material flux.

Excess Mn can be used as an indicator of advective mixing of the water near the seafloor because it is controlled by the diffusion of soluble Mn^{2+} produced via MnO_2 reduction in the sediment, mobilization into the water column, subsequent oxidation into particles, and settling (Yeats et al., 1979; Davison et al., 1982; Kim et al., 2017). Both the content and flux of excess Mn were several times greater at 4950 m when compared with 4500 m. Despite the difference in magnitude of the excess Mn contents at these two depths, its temporal variations at the two depths were similar at both (Fig. 3). The excess Mn could be derived from either local resuspension or transported within the BNL from the distant seafloor.

Around the study site, surface sediment is composed mostly of lithogenic material (92%) and opal (7.6%), with minor contributions from organic carbon (0.5%) and $CaCO_3$ (0.1%; Kim et al., 2015). Under the assumption that the particle composition does not change during the resuspension process, the contribution of resuspended sediment to sinking particles can be estimated from the lithogenic material content. First, lithogenic material derived from sediment resuspension ($Litho_{resusp}$) was calculated by subtracting the atmospheric dust deposition from the total lithogenic material content in the sinking particles ($Litho_{resusp}$ = Total lithogenic material in trap−dust deposition). Then the contribution of each component derived from sediment resuspension was estimated by multiplication of the ratio of each component to lithogenic material in the surface sediment to $Litho_{resusp}$. The contribution of resuspended opal and POC to each corresponding fraction of the sinking particles was 0.6% and 0.1% (arithmetic mean), respectively, at 4500 m. The values were somewhat larger at 4950 m, 2.9% and 0.7%, for opal and POC, respectively. In total, resuspended sediment accounted for 2.4% and 13% of the total sinking particles in the flux- and duration-weighted averages. Resuspension of $CaCO_3$ was not considered because of its extremely low concentration in the sediment. In addition, most of the $CaCO_3$ flux at this site is derived from foraminifera (Kim et al., 2019). Strong currents, exceeding 10 cm s^{-1}, are necessary for resuspension of foraminifera (Yamasaki and Oda, 2003), and they are thus less susceptible to resuspension.

At continental margins, if it is significantly less than the value for dissolved inorganic carbon (DIC) and/or freshly produced POC in the surface water, the $\Delta^{14}C$ values of sinking POC can be used as a reliable indicator of the relative contribution of aged, allochthonous organic

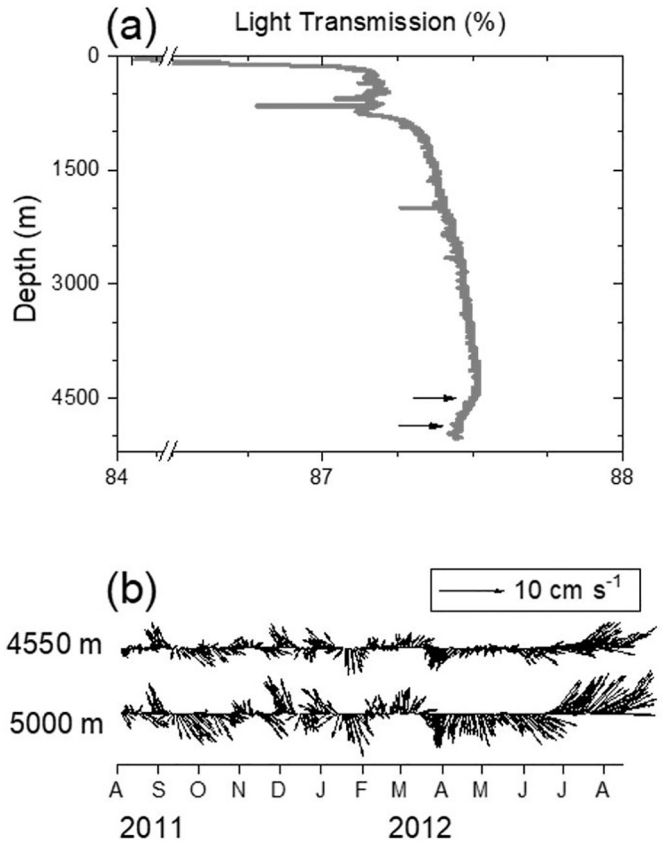

Fig. 4. (a) Light transmission obtained during July 2010. A decrease in light transmission is observed in the bottom ~300 m. Sampling depths of sediment traps are indicated by the arrows. (b) Current direction and magnitude at 4550 and 5000 m measured at the mooring site.

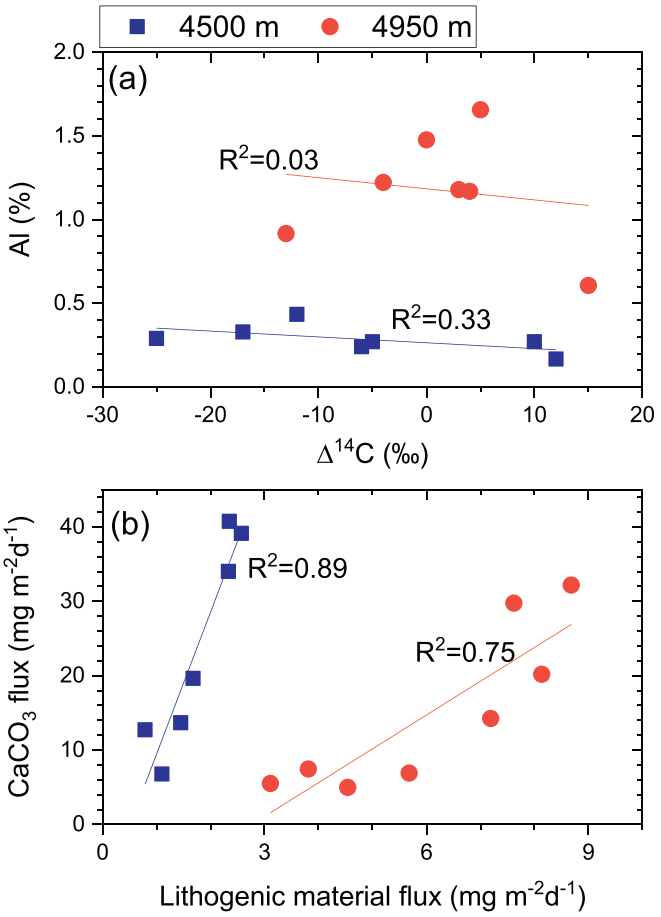

Fig. 5. Relationships between (a) the $\Delta^{14}C$ value of sinking POC and the Al content (%) and (b) the fluxes of $CaCO_3$ and lithogenic material.

carbon to sinking POC (Hwang et al., 2010; Kim et al., 2020). At our site, the contribution of POC from sediment resuspension is so low (<1%) as estimated earlier based on the lithogenic material content that its effect on the $\Delta^{14}C$ values of sinking POC should be very small (<5‰). However, significantly low $\Delta^{14}C$ values were observed at both depths and no significant correlation was observed between the lithogenic material content and $\Delta^{14}C$ values (Fig. 5). The reason for the unexpectedly low $\Delta^{14}C$ values is not clear. One potential cause of the large variation in $\Delta^{14}C$ values is the ENSO cycle (Kim et al., 2010, 2011, 2019). During La Niña events, enhanced upwelling brings up the deep water with low $\Delta^{14}C$ values to the surface. Although we made no direct measurement of the $\Delta^{14}C$ values of dissolved inorganic carbon at our site, the temporal fluctuation in the $\Delta^{14}C$ values of the Galapagos coral related to the ENSO cycle was shown to be as large as ~40‰ (Guilderson and Schrag, 1998). A La Niña event occurred in 2010/2011; consequently, low $\Delta^{14}C$ values in the surface water DIC are to be expected. During the weak La Niña during the winter of 2016, the $\Delta^{14}C$ values of DIC in the upper 50 m of the eastern Pacific (7–15°N, 110°W; $n = 8$) ranged between 8.9‰ and 34‰ (Key and McNichol, 2020). Temporal variations in the $\Delta^{14}C$ values of surface water DIC can be as large as 32‰ at a given location (49‰ and 81‰, at Station M at 34.8°N 123°W; data retrieved from the Global Ocean Data Analysis Project for Carbon; Masiello et al., 1998; Key et al., 2004; Druffel et al., 2010). Therefore, caution should be applied when using radiocarbon-based estimations of resuspended POC input for sites where potentially large variability is suspected.

4.2. *Scavenging of resuspended sediment by biogenic particles*

At the abyssal plain site of Station KOMO, the bottom current was weak and did not exhibit any correlation with the properties related to sediment resuspension. Instead, the lithogenic material flux showed a strong positive correlation with the biogenic flux (Fig. 5). The $CaCO_3$ flux can be used to represent the biogenic particle flux because of the very low $CaCO_3$ concentration found in surface sediments. The $CaCO_3$ flux showed a correlation with the lithogenic material flux with R^2 values of 0.89 and 0.75 at 4500 m and 4950 m, respectively. A good correlation between the fluxes of Al and POC in the sinking particle samples was also observed in the Sargasso Sea, implying incorporation of lithogenic particles into biological particles (Chester and Jickells, 2012). Aluminosilicate minerals are particle-reactive and removed by passive scavenging onto particulate material (Goldberg, 1954; Orians and Bruland, 1985; Bruland and Lohan, 2003). We suggest that the fine particles derived from sediment resuspension exist at a background level in the BNL throughout the year, and that they are scavenged by fresh biological particles sinking from the overlying water column during the high flux period. The temporal development of the lithogenic material flux shows that the flux increases and decreases following variations in the biogenic particle flux between December and April. The low lithogenic material flux seen from May onwards implies that it takes some time for the background particle concentration to recover following a scavenging event. At 4500 m, most of the resuspended sediment appears to be scavenged by the high biogenic flux event. From May to July, the lithogenic material flux was virtually identical to the atmospheric dust deposition rate (Fig. 3).

5. Conclusion

Based on our examination of the biogenic and lithogenic particle composition and radiocarbon content in sinking POC, we have gained an

insight into the sediment resuspension and its contribution to sinking particles on the deep abyssal plain. Even in the middle of the open ocean, the BNL was present (~300 m thick), and the sediment derived lithogenic material flux was elevated compared with the layer immediately above, and the particulate Mn flux was affected by the efflux from the sediment. Temporal variations in the lithogenic material flux imply that resuspended particles existed at a background concentration in the BNL throughout the year and are scavenged by sinking biogenic particles especially during the high flux period. In contrast to the continental margin settings, the $\Delta^{14}C$ value of sinking POC is not an effective indicator of sediment resuspension in the open ocean setting, especially where variations in the $\Delta^{14}C$ value of DIC in the surface water can be large because of the effects of the ENSO cycle.

Author contributions

HJK, SJJ and JH designed the study. MK, HJK, AK, and CMK performed the sample analysis and/or data interpretation. MK, HJK and JH led the writing of the paper. All co-authors contributed to the writing via discussion of the manuscript.

Declaration of Competing Interest

The authors declare that they have no known competing financial interests or personal relationships that could have appeared to influence the work reported in this paper.

Acknowledgements

We thank the captain and crew of the R/V *Onnuri* for help at sea; Young June Kim at KIOST for the transmissometer data; staffs at the Korea Basic Science Institute for metal analysis; and staffs at NOSAMS WHOI and ETH Zürich for carbon isotopic analysis. This research was supported by the KIOST internal project (PE99923), and contributed to the environmental baseline studies associated with the polymetallic manganese nodules exploration of the Republic of Korea (Ministry of Oceans and Fisheries R&D grant number: 20160099).

References

Acker, J.G., Leptoukh, G., 2007. Online analysis enhances use of NASA Earth science data. EOS Trans. Amer. Geophys. Union 88, 14–17.

Armstrong, R.A., Lee, C., Hedges, J.I., Honjo, S., Wakeham, S.G., 2001. A new, mechanistic model for organic carbon fluxes in the ocean based on the quantitative association of POC with ballast minerals. Deep-Sea Res. II 49, 219–236.

Blackburn, M., Laurs, R., Owen, R., Zeitzschel, B., 1970. Seasonal and areal changes in standing stocks of phytoplankton, zooplankton and micronekton in the eastern tropical Pacific. Mar. Biol. 7, 14–31.

Bruland, K.W., Lohan, M.C., 2003. Controls of trace metals in seawater. In: Holland, H. D., Turekian, K.K. (Eds.), Treatise on Geochemistry, vol. 6. Elsevier-Pergamon, Oxford, U. K., pp. 23–47. https://doi.org/10.1016/B0- 44708-043751-6/06105-3

Buesseler, K.O., 1998. The decoupling of production and particulate export in the surface ocean. Glob. Biogeochem. Cycles 12, 297–310. https://doi.org/10.1029/97GB03366.

Buesseler, K.O., Boyd, P.W., 2009. Shedding light on processes that control particle export and flux attenuation in the twilight zone of the open ocean. Limnol. Oceanogr. 54, 1210–1232.

Buesseler, K.O., Trull, T.W., Steinberg, D.K., Silver, M.W., Siegel, D.A., Saitoh, S.-I., Lamborg, C.H., Lam, P.J., Karl, D.M., Jiao, N., 2008. VERTIGO (VERtical Transport In the Global Ocean): a study of particle sources and flux attenuation in the North Pacific. Deep-Sea Res. II 55, 1522–1539. https://doi.org/10.1016/j.dsr2.2008.04.024.

Chester, R., Jickells, T., 2012. Down-column fluxes and the benthic boundary layer. In: Marine Geochemistry. John Wiley, New York, NY, pp. 253–270.

Christl, M., Vockenhuber, C., Kubik, P.W., Wacker, L., Lachner, J., Alfimov, V., Synal, H.-A., 2013. The ETH Zürich AMS facilities: performance parameters and reference materials. Nucl. Instrum. Methods Phys. Res. 294, 29–38.

Davison, W., Woof, C., Rigg, E., 1982. The dynamics of iron and manganese in a seasonally anoxic lake; direct measurement of fluxes using sediment traps. Limnol. Oceanogr. 27, 987–1003.

Druffel, E.R.M., Beaupre, S., Griffin, S., Hwang, J., 2010. Variability of dissolved inorganic radiocarbon at a surface site in the Northeast Pacific Ocean. Radiocarbon 52, 1150–1157. https://doi.org/10.1017/S0033822200046221.

Duce, R., 2014. A dusty planet. Oceanography 27, 66–68. JSTOR. www.jstor.org/stable/24862120.

Ducklow, H.W., Steinberg, D.K., Buesseler, K.O., 2001. Upper ocean carbon export and the biological pump. Oceanography 14, 50–58. https://doi.org/10.5670/oceanog.2001.06.

El-Sayed, S.Z., Taguchi, S., 1979. Phytoplankton standing crop and primary productivity in the tropical Pacific. In: Bischoff, J.L., Piper, D.Z. (Eds.), Marine Geology and Oceanography of the Pacific Manganese Nodule Province. Springer, Pergamon, New York, pp. 241–286.

Gardner, W.D., Souchard, J.B., Hollister, C.D., 1985. Sedimentation, resuspension and chemistry of particles in the northwest Atlantic. Mar. Geol. 65, 199–242.

Gardner, W.D., Richardson, M.J., Mishonov, A.V., 2018. Global assessment of benthic nepheloid layers and linkage with upper ocean dynamics. Earth Planet. Sci. Lett. 482, 126–134. https://doi.org/10.1016/j.epsl.2017.11.008.

Goldberg, E.D., 1954. Marine geochemistry: 1. Chemical scavengers of the sea. J. Geol. 62, 249–265.

Guilderson, T.P., Schrag, D.P., 1998. Abrupt shift in subsurface temperatures in the tropical Pacific associated with changes in El Niño. Science 281 (5374), 240–243. https://doi.org/10.1126/science.281.5374.240.

Hedges, J.I., Stern, J.H., 1984. Carbon and nitrogen determinations of carbonate-containing solids. Limnol. Oceanogr. 29, 657–663.

Hollister, C., McCave, I., 1984. Sedimentation under deep-sea storms. Nature 309, 220–225.

Honda, M.C., Kusakabe, M., Nakabayashi, S., Katagiri, M., 2000. Radiocarbon of sediment trap samples from the Okinawa trough: lateral transport of 14C-poor sediment from the continental slope. Mar. Chem. 68, 231–247.

Honjo, S., Dymond, J., Collier, R., Manganini, S.J., 1995. Export production of particles to the interior of the equatorial Pacific Ocean during the 1992 EqPac experiment. Deep Sea Res. II 42, 831–870. https://doi.org/10.1016/0967-0645(95)00034-N.

Hwang, J., Druffel, E.R.M., Eglinton, T.I., 2010. Widespread influence of resuspended sediments on oceanic particulate organic carbon: Insights from radiocarbon and aluminum contents in sinking particles. Glob. Biogeochem. Cycles. 24.

Inthorn, M., Mohrholz, V., Zabel, M., 2006. Nepheloid layer distribution in the Benguela upwelling area offshore Namibia. Deep-Sea Res. I 53, 1423–1438. https://doi.org/10.1016/j.dsr.2006.06.004.

Karakaş, G., Nowald, N., Blaas, M., Marchesiello, P., Frickenhaus, S., Schlitzer, R., 2006. High-resolution modeling of sediment erosion and particle transport across the northwest African shelf. J. Geophys. Res. 111.

Key, R. M., and McNichol, A. P., 2020. DIC-14C data from P18 cruise legs 1 and 2 in 2016/17. expo code 33RO20161119. doi:https://doi.org/10.7289/v5cv4g1w.

Key, R.M., Kozyr, A., Sabine, C.L., Lee, K., Wanninkhof, R., Bullister, J.L., Feely, R.A., Millero, F.J., Mordy, C., Peng, T.-H., 2004. A global ocean carbon climatology: results from Global Data Analysis Project (GLODAP). Glob. Biogeochem. Cy. 18, GC4031 https://doi.org/10.1029/2004GC002247.

Kim, H.J., Hyeong, K., Yoo, C.M., Chi, S.-B., Khim, B.-K., Kim, D., 2010. Seasonal variations of particle fluxes in the northeastern equatorial Pacific during normal and weak El Niño periods. Geosci. J. 14, 415–422.

Kim, H.J., Kim, D., Yoo, C.M., Chi, S.-B., Khim, B.K., Shin, H.-R., Hyeong, K., 2011. Influence of ENSO variability on sinking-particle fluxes in the northeastern equatorial Pacific. Deep-Sea Res. I 58, 865–874.

Kim, H.J., Kim, D., Hyeong, K., Hwang, J., Yoo, C.M., Ham, D.J., Seo, I., 2015. Evaluation of resuspended sediments to sinking particles by benthic disturbance in the Clarion-Clipperton nodule fields. Mar. Georesour. Geotec. 33, 160–166.

Kim, H.J., Kim, T.W., Hyeong, K., Yeh, S.W., Park, J.Y., Yoo, C.M., Hwang, J., 2019. Suppressed CO_2 outgassing by an enhanced biological pump in the Eastern Tropical Pacific. J. Geophys. Res. 124 (11), 7962–7973.

Kim, M., Hwang, J., Rho, T.K., Lee, T., Kang, D.J., Chang, K.I., Noh, S., Joo, H.T., Kwak, J.H., Kang, C.K., Kim, K.R., 2017. Biogeochemical properties of sinking particles in the southwestern part of the East Sea (Japan Sea). J. Mar. Syst. 167, 33–42.

Kim, M., Hwang, J., Eglinton, T.I., Druffel, E.R.M., 2020. Lateral particle supply as a key vector in the oceanic carbon cycle. Glob. Biogeochem. Cy. 34, e2020GB006544.

Komada, T., Anderson, M.R., Dorfmeier, C.L., 2008. Carbonate removal from coastal sediments for the determination of organic carbon and its isotopic signatures, $\delta^{13}C$ and $\Delta^{14}C$: comparison of fumigation and direct acidification by hydrochloric acid. Limnol. Oceanogr. Methods 6, 254–262.

Lampitt, R., 1985. Evidence for the seasonal deposition of detritus to the deep-sea floor and its subsequent resuspension. Deep-Sea Res. I 32, 885–897.

Marsay, C.M., Sanders, R.J., Henson, S.A., Pabortsava, K., Achterberg, E.P., Lampitt, R.S., 2015. Attenuation of sinking particulate organic carbon flux through the mesopelagic ocean. Proc. Natl. Acad. Sci. U. S. A. 112, 1089–1094.

Martin, J.H., Knauer, G.A., Karl, D.M., Broenkow, W.W., 1987. VERTEX: carbon cycling in the northeast Pacific. Deep-Sea Res. I 34, 267–285.

Masiello, C.A., Druffel, E.R.M., Bauer, J.E., 1998. Physical controls on dissolved inorganic radiocarbon variability in the California current. Deep-Sea Res. II 45, 617–642.

McCave, I., Hall, I.R., 2006. Size sorting in marine muds: processes, pitfalls, and prospects for paleoflow-speed proxies. Geochem. Geophys. Geosyst. 7 https://doi.org/10.1029/2006GC001284.

McIntyre, C.P., Wacker, L., Haghipour, N., Blattmann, T.M., Fahrni, S., Usman, M., Eglinton, T.I., Synal, H.-A., 2017. Online ^{13}C and ^{14}C gas measurements by EA-IRMS–AMS at ETH Zürich. Radiocarbon 59 (3), 893–903. https://doi.org/10.1017/RDC.2016.68.

McNichol, A., Osborne, E., Gagnon, A., Fry, B., Jones, G., 1994. TIC, TOC, DIC, DOC, PIC, POC-unique aspects in the preparation of oceanographic samples for ^{14}C-AMS. Nucl. Instrum. Meth. B 92, 162–165.

Orians, K.J., Bruland, K.W., 1985. Dissolved aluminium in the central North Pacific. Nature 316 (6027), 427–429. https://doi.org/10.1038/316427a0.
Otosaka, S., Tanaka, T., Togawa, O., Amano, H., Karasev, E.V., Minakawa, M., Noriki, S., 2008. Deep sea circulation of particulate organic carbon in the Japan Sea. J. Oceanogr. 64, 911–923.
Pennington, J.T., Mahoney, K.L., Kuwahara, V.S., Kolber, D.D., Calienes, R., Chavez, F.P., 2006. Primary production in the eastern tropical Pacific: a review. Prog. Oceanogr. 69, 285–317. https://doi.org/10.1016/j.pocean.2006.03.012.
Taylor, S., 1964. Abundance of chemical elements in the continental crust: a new table. Geochim. Cosmochim. Acta 28, 1273–1285.
Yamasaki, M., Oda, M., 2003. Sedimentation of planktonic foraminifera in the East China Sea: evidence from a sediment trap experiment. Mar. Micropaleontol. 49, 3–20.
Yeats, P., Sundby, B., Bewers, J., 1979. Manganese recycling in coastal waters. Mar. Chem. 8, 43–55.